ISSN1027-5495. Functional Materials, 25, No.2 (2018), p. 282-288
doi:https://doi.org/10.15407/fm25.02.282 © 2018 — STC "Institute for Single Crystals"

Effects of metal ion-doping on the characteristics and photocatalytic activities of TiO_2 nanotubes

Shaona Wang, Rongfang Yuan, Beihai Zhou, Huanhuan Guan

Beijing Key Laboratory of Resource-oriented Treatment of Industrial Pollutants, Department of Environment Engineering, School of Civil and Environmental Engineering, University of Science and Technology Beijing, Beijing 100083

Received January 25, 2018

Ion-doped TiO_2 nanotubes were synthesized via a hydrothermal method and characterized by transmission electron microscopy, X-ray diffraction, X-ray photoelectron spectroscopy and specific surface areas. The binding energies of Cu^{2+}, V^{2+}, and Zn^{2+} indicated that the doping ions existed as Cu^{2+}, V^{5+}, and Zn^{2+}, respectively. With the increase of the calcination temperature, the intensity of the anatase phase decreased and the BET surface area decreased. The extent of anatase phase increased with the increasing the calcination temperature, and then decreased. The highest catalytic activity for the un-doped TiO_2 nanotubes was observed at a calcination temperature of 500 °C, with a Rhodamine B (RB) removal efficiency of 98.1%. The removal efficiency of RB was 98.2% when Cu^{2+}-doped catalyst calcined at 450 °C was added, 0.1% higher than the un-doped TiO_2 nanotubes. The highest photocatalytic activity was obtained in the presence of Zn^{2+}-doped catalyst calcined at 550 °C, where 98.7% of RB was removed.

Keywords: nanotubes; metal ions-doped; Rhodamine B; photocatalytic oxidation

Методом электронной микроскопии, рентгеновской дифракции, рентгеновской фотоэлектронной спектроскопии изучены ионо-легированные нанотрубки TiO_2 синтезированные гидротермическим методом .Энергии связи Cu^{2+}, V^{2+} и Zn^{2+} показали, что легирующие ионы существуют как Cu^{2+}, V^{5+} и Zn^{2+}, соответственно. С увеличением температуры прокаливания интенсивность фазы анатаза уменьшалась и площадь поверхности по БЭТ уменьшалась. Степень фазы анатаза увеличивалась с увеличением температуры прокаливания, а затем уменьшалась. Наибольшая каталитическая активность для нелегированных нанотрубок TiO_2 наблюдалась при температуре прокаливания 500 ° С с эффективностью удаления Rhodamine B (RB) 98,1%. Эффективность удаления RB составляла 98,2%, когда катализатор, легированный Cu^{2+}, прокаленный при 450 ° С, был добавлен на 0,1% выше, чем не легированные нанотрубки TiO_2. Наибольшая фотокаталитическая активность получена в присутствии катализатора, легированного Zn^{2+}, прокаленного при 550 °С, где было удалено 98,7% RB.

Вплив іонного легування металів на характеристики і фотокаталітичні активності нанотрубок TiO_2. *Shaona Wang, Rongfang Yuan, Beihai Zhou, Huanhuan Guan*

Методом електронної мікроскопії, рентгенівської дифракції, рентгенівської фотоелектронної спектроскопії вивчено іоно-леговані нанотрубки TiO_2 синтезовані гідротермічним методом .Енергії зв'язку Cu^{2+}, V^{2+} і Zn^{2+} показали, що легуючі іони існують як Cu^{2+}, V^{5+} і Zn^{2+}, відповідно. Зі збільшенням температури прожарювання інтенсивність фази анатазу зменшувалася і площа поверхні по БЕТ зменшувалася. Ступінь фази анатазу збільшувалася зі збільшенням температури прожарювання, а потім зменшувалася. Найбільшу каталітична активність для нелегованих нанотрубок TiO_2 спостерігалася при температурі прожарювання 500 °С з ефективністю видалення Rhodamine B (RB) 98,1%. Ефективність видалення RB становила 98,2%, коли каталізатор, легований Cu^{2+}, прожарений при 450 ° С, був доданий на 0,1% вище, чим не леговані нанотрубки TiO_2. Найбільша фотокаталітичну активність отримано у присутності каталізатора, легованого Zn^{2+}, прожареного при 550 °С, де видалено 98,7% RB.

1. Introduction

Rhodamine B (RB) is a representative of xanthene cationic dyes and is known for its stability [1] It is harmful if swallowed and can cause irritation to the skin, eyes and respiratory tract. Photocatalytic oxidation is highly efficient in generating ·OH for the degradation of the pollutants [2].

The choice of photocatalysis is essential in RB removal, and TiO_2 is a good candidate, because TiO_2-photocatalyzed reactions are non-selective oxidation processes at the level of micrograms per litre, and the use of TiO_2 is effective for inactive substrates [3]. The photocatalytic performance of TiO_2 depends on its crystal structure, particle size as well as effective surface area, and therefore with the use of nano-sized TiO_2 the number of particles per unit area is increased enhancing its photocatalytic activity in the UV light [4, 5]. Compared with its powder form, TiO_2 nanotubes have a larger BET surface area (S_{BET}), which is advantageous in one-electron oxidation during photocatalytic reactions [6]. But, the relatively large bandgap of TiO_2 (3.2 eV) limits the efficiency of photocatalytic reactions because of the high recombination rate of photogenerated electrons and holes [7]. Various attempts have been made to modify TiO_2 to enhance its photocatalytic activity by coupling with other materials, such as semiconductor materials, metal ions [7], dyes and non-metal elements. These materials can form the energies of the intermediate states in the band gap. It is generally considered that the substitution for Ti^{4+} in the TiO_2 lattice by certain metal ions creates impurity energy levels within the band gap, which may induce the activity of TiO_2 [8] and act as electron trapper to inhibit the recombination of photo-generated electron–hole pairs [9]. Special attention has been recently focused on the investigation of the effect induced by transition metal dopants on the physicochemical properties of TiO_2 and on the consequent change in photoactivity.

In this study, we investigated the effect of metal ion-doping on the photocatalytic activity of TiO_2 nanotubes for RB removal via the UV/TiO_2 method. Three types of metal ions, namely, Cu^{2+}, V^{5+}, and Zn^{2+}, were investigated, and Zn^{2+} was observed to be the optimum ion type. Analyses of the TiO_2 nanotubes were conducted to determine the factors that affect the photocatalytic activities of the catalysts.

2. Materials and methods

2.1 Materials

P-25 TiO_2 was provided by the Degussa Corporation (Richfield Park, New Jersey). The powder has an S_{BET} of 50 $m^2 \cdot g^{-1}$, an average crystallite size of 21 nm, and a crystal structure of 80% anatase and 20% rutile. RB (A.R.) was purchased from Beijing Chemical Reagent Company.

A photocatalytic reactor (60 mm diameter and 750 mm length), which was equipped with a 37 W 254 nm UV lamp (15 mm Dia. and 793 mm Lth.) purchased from Haili Lighting Equipment Company (Beijing), was used in this experiment. O_2 was generated by an oxygenator (Yao, Beijing), and was guided into the photocatalytic reactor through the bottom port. The samples were acquired from the sampling port in the middle of the reactor.

2.2. Preparation of TiO_2 nanotubes

One gram of P-25 TiO_2 was added to 16 mL of a 10 $mol \cdot L^{-1}$ NaOH aqueous solution in a Teflon vessel. The mixture was then stirred for 2 h at room temperature. The mixture was then heated at 110 °C for 24 h in an oven, and cooled to room temperature in air. The as-prepared precipitate ($Na_2Ti_3O_7$) was washed with distilled water to achieve a pH of 7 and then subsequently dispersed in a 0.1 $mol \cdot L^{-1}$ HCl aqueous solution. After ultrasonication for 30 min, the precipitate was continuously washed to achieve a pH of 7 and then dried at 60 °C. The nanotubes were prepared by calcining the precipitate at corresponding temperatures (450 °C, 500 °C, 550 °C, and 600 °C) for 2 h.

The ion-doped TiO_2 nanotubes were prepared using the aforementioned process in the presence of added metal salts to obtain a doping level of about 1.0%. The following metal salts were used as precursors for dopant ions: $CuCl_2 \cdot 2H_2O$, NH_4VO_3, and $ZnCl_2$. The corresponding amounts added to the 10 $mol \cdot L^{-1}$ NaOH solution were 0.0213, 0.0146, and 0.0170 g, respectively. All dopant concentrations mentioned in this study are the nominal atomic values based on the assumption of quantitative dopant incorporation.

2.3 Characterization of TiO_2 nanotubes

X-ray diffraction (XRD) patterns were collected using a Rigaku Dmax-RB diffractometer (Tokyo, Japan). The surface elemental composition of TiO_2 was recorded via X-ray photoelectron spectroscopy (XPS, AXIS ULTRA^{DLD}, Kratos Analytical, UK). Transmission electron microscopy (TEM) images were obtained using a HITACHI HT-7700 electron microscope (Tokyo, Japan). S_{BET} was measured using the Quadrasorb SI-MP apparatus (Quantachrome Instrument, USA). Diffuse reflectance spectroscopy (DRS) analyses were performed using a HITACHI U-3010 UV-vis scanning spectrophotometer (Tokyo, Japan).

Table1. Catalytic properties of the TiO_2 nanotube samples.

Calcination temperature /°C	Weight fractions of anatase phase (%)				Indirect energy band gap/ (eV)				BET surface areas/($m^2 \cdot g^{-1}$)			
	450	500	550	600	450	500	550	600	450	500	550	600
un-doped	78.8	82.6	83.4	76.9	3.26	3.24	3.24	3.22	237	169	123	99
Cu^{2+}-doped	83.8	84.9	91.3	86.3	3.23	3.22	3.21	3.15	190	132	99	85
V^{5+}-doped	61.0	90.6	85.3	86.5	3.21	3.21	3.20	3.20	264	172	123	102
Zn^{2+}-doped	74.1	80.3	81.5	84.8	3.25	3.21	3.19	3.18	211	153	134	110

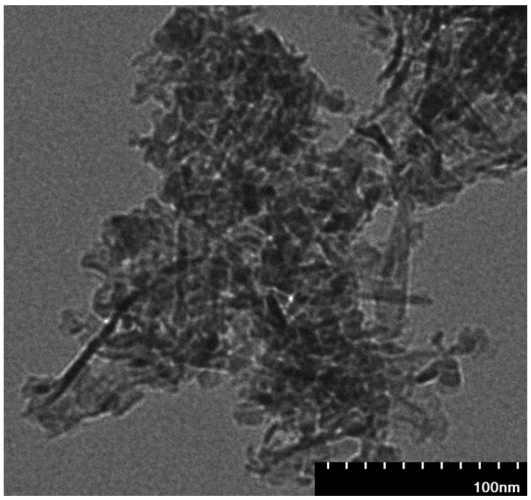

Fig. 1. TEM images of Zn^{2+}-doped TiO_2 nanotubes calcined at 550 °C.

2.4. Photocatalytic activity tests

Aqueous slurries were prepared by adding 0.15 g of TiO_2-based photocatalyst to 1500 mL of 20 mg·L^{-1} RB aqueous solution at pH 7. The aqueous slurries were bubbled with O_3 (1 L·min^{-1}) and irradiated with a 254 nm UV lamp. Every 10 min, a 20 mL sample was acquired and centrifuged at 2000 rpm. The concentration of RB was determined using a UV-visible spectrophotometer (DR5000, Hach) at 500 nm.

3 Results and Discussion

3.1. Characterization of photocatalysts

Transmission electron microscopy was performed to observe the morphology of the catalyst. Figure 1 shows the morphologies of Zn^{2+}-doped TiO_2 nanotubes calcined at 550 °C. The TiO_2 nanotube was successfully synthesized. Other ion-doped nanotubes shared a similar morphology.

Figures 2(a) and 2(b) show the XRD patterns of the un-doped and ion-doped TiO_2 nanotubes, respectively. The weight fractions of anatase in the anatase-rutile mixtures in the samples were calculated using Eq.1 [10].

$$f = \frac{1}{1 + 1.265\frac{I_R}{I_A}} \quad (1)$$

Where f is the weight fractions of anatase in the mixtures, and I_R and I_A are the maximum X-ray diffraction peak intensities of rutile phase (110) and anatase phase (101), respectively. Table 1 lists the weight fractions of anatase in various samples.

Fig. 2 and Table 1 show that both anatase and rutile phases existed in the TiO_2 nanotubes. The characteristic peaks of the (101) crystal plane of anatase and the (110) crystal

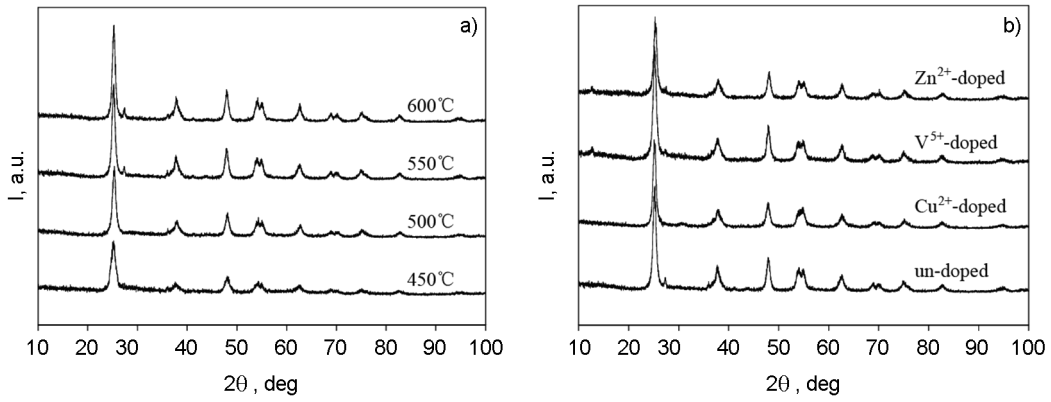

Fig. 2 . XRD patterns of the TiO_2 nanotubes. (a) un-doped TiO_2; (b) ion-doped TiO_2 with different doped ions calcined at 550 °C.

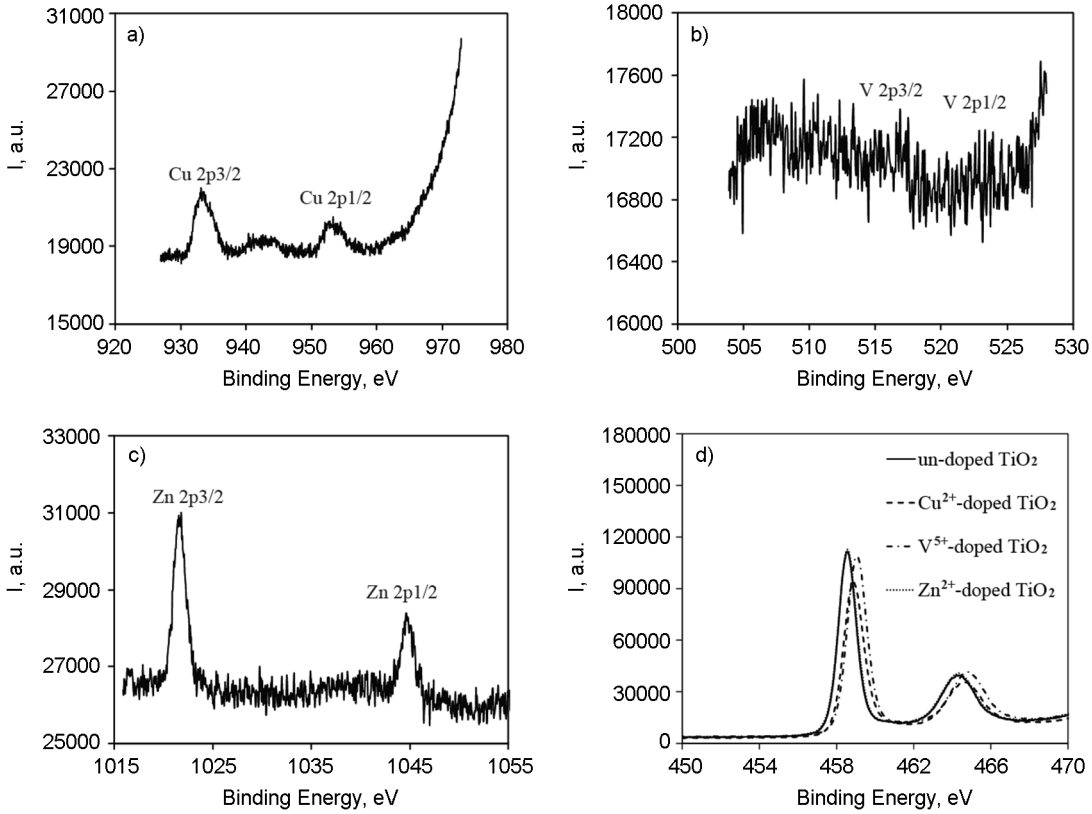

Fig. 3. XPS spectra of the TiO_2 nanotubes: (a) Cu^{2+}; (b) V^{2+}; (c) Zn^{2+}; (d) Ti^{2+}.

plane of rutile were located at about 25.3° and 27.4°, respectively. When the calcination temperature was increased, the intensity of the anatase phase decreased, whereas that of the rutile phase increased. Compared with those of un-doped TiO_2, the Bragg angles of the (101) peak position of the ion-doped TiO_2 shifted to lower angles (25.34, 25.18, 25.16 and 25.26 for un-doped, Cu^{2+}-doped, V^{5+}-doped and Zn^{2+}-doped TiO_2, respectively), and the anatase peak intensity decreased. These results occurred because the crystallite had numerous crystal planes caused by ion doping; thus, such crystallite could not be considered as an ideal crystal. Furthermore, the dopant ions could substitute Ti^{4+} in the TiO_2 nanotubes lattice, which resulted in the deformation of the crystal lattice. As a result, a broadening diffraction peak and a decreasing peak intensity were observed.

Some ions were partially dispersed in the bulk of TiO_2 nanotubes [11]. The metallic oxides from other doped ions might also be formed on the surface of TiO_2. These oxides were not observed in the XRD patterns because their metal sites (0.5-2.0 wt.%) were expected to be below the visibility limit of X-ray analysis [12].

The XPS analysis was performed to determine the surface composition and the chemical state of the elements in the ion-doped TiO_2 nanotubes calcined at 550 °C (Fig. 3a). The binding energies of Cu^{2+}, V^{2+}, and Zn^{2+} indicate that the doping ions existed as Cu^{2+}, V^{5+}, and Zn^{2+} in the TiO_2 crystal lattice.

Fig. 3d shows that binding energies of 458.15 eV to 459.00 eV for TiO_2 nanotubes correspond to the peaks of $Ti^{2+}3/2$, whereas binding energies of 464.05 eV to 464.90 eV correspond to $Ti^{2+}1/2$. The binding energy of Ti^{2+} indicates that Ti was incorporated into the lattice of TiO_2 as Ti^{4+}. When additional ions are introduced into the lattice, interaction between the outer-shell orbitals of these ions and the energy states in the bands creates impurity levels and changes the band structures. The Ti^{2+} binding energy of the ion-doped TiO_2 nanotubes increased compared with that of pure TiO_2 because the electrons in the conduction band of TiO_2 are transferred to the doped metal ions on the surface of TiO_2, which resulted in a decrease in the outer electron cloud density of Ti ions [13]. The ions, which have high oxidation states, decrease the energy of both the valence band maximum and the conduction band minimum because more oxygen ions are needed for charge compensation. The high occupancy of *d*-orbitals lowers the energy of the *d* states, thus moving the energy levels away from the conduction band and contributing to the valence band maximum [14].

Table 2. The first order kinetics equation fitting of the TiO_2 nanotube samples

Parameter		Equation	R2
Cu-doped TiO_2	450 °C	Y=15.093ln(x)+43.558	0.7914
	500 °C	Y=18.595ln(x)+29.265	0.8439
	550 °C	Y=22.217ln(x)+15.158	0.8449
	600 °C	Y=25.7ln(x)+2.0518	0.8732
Zn-doped TiO_2	450 °C	Y=34.301ln(x)+7.4218	0.8713
	500 °C	Y=20.472ln(x)+23.192	0.838
	550 °C	Y=15.003ln(x)+43.851	0.8402
	600 °C	Y=19.856ln(x)+25.673	0.8508
V-doped TiO_2	450 °C	Y=21.114ln(x)+18.398	0.8682
	500 °C	Y=16.391ln(x)+36.875	0.8313
	550 °C	Y=13.319ln(x)+49.558	0.8614
	600 °C	Y=16.05ln(x)+39.118	0.8452

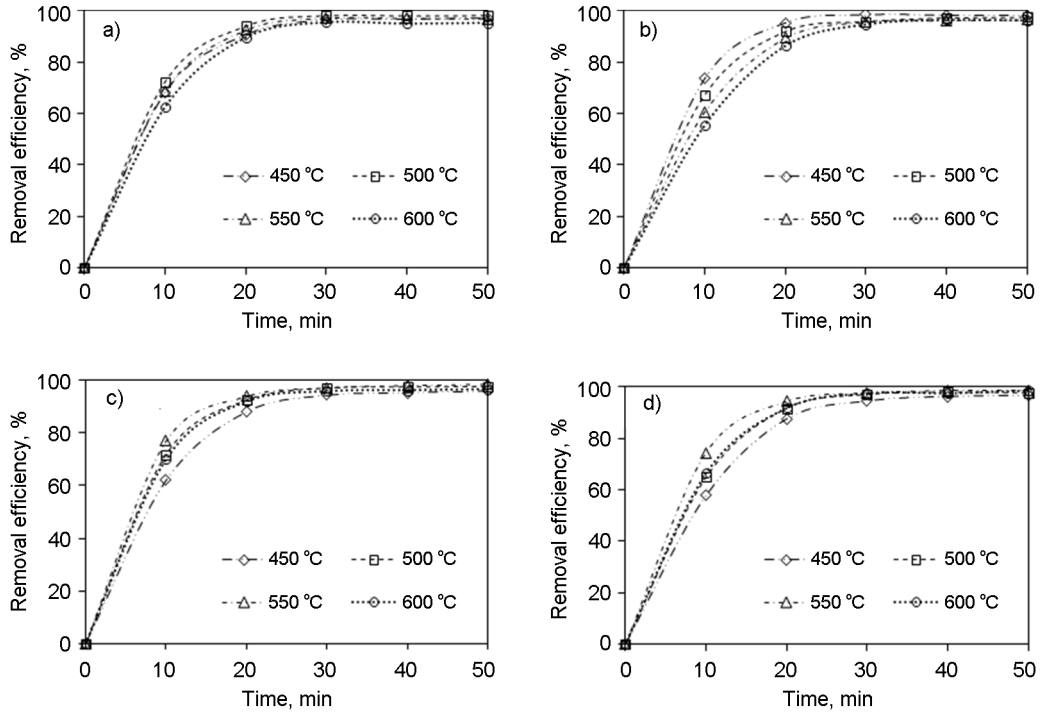

Fig. 4. Removal of 20 mg·L^{-1} RB in the presence: of different TiO_2 nanotubes (a) un-doped TiO_2; (b) Cu^{2+}-doped TiO_2; (c) V^{5+}-doped TiO_2; (d) Zn^{2+}-doped TiO_2.

The catalytic efficiencies of the TiO_2 nanotubes are related to the S_{BET} of the catalyst [15]./ As summarized in Tabl. 1, the S_{BET} of TiO_2 nanotubes decreased with increasing calcination temperature. The decrease in S_{BET} could be attributed to the aggregation of nanotubes, which resulted in a closely coagulated structure [16]. The S_{BET} of ion-doped TiO_2 nanotubes was smaller than that of un-doped TiO_2 nanotubes. The S_{BET} decreased when metal ions were doped because of partial pore blockages and framework defects [11] .

The S_{BET} of TiO_2 nanotubes was significantly larger than that of P-25 TiO_2. This finding is attributed to the inner and outer surfaces of the layered-tubular structure, which is one of the special qualities of this catalyst [17].

The UV-vis DRS analysis was performed on the catalysts to obtain the energy band gaps (E_g). TiO_2 nanotubes have an indirect band gap, and the plots relation was used:

$$F(R_\infty)h\gamma = A(\mathrm{h}\gamma\text{-}E_g)^2 \qquad (2)$$

Where $F(R)$ is the Kubelka-Munk (K-M) function, h is the Planck constant, and γ is the frequency. The value of $F(R)$ can be estimated using the K-M formula:

$$F(R_\infty) = K / S = \frac{(1-R_\infty)^2}{2R_\infty} \quad (3)$$

Where R_∞ is the diffuse reflectance. The plots of E_g were deduced from the intersection of the linear portion extrapolation with the energy axis. Table 1 shows the E_g of the catalysts.

The E_g decreased with increasing calcination temperature. This trend occurred because the E_g of rutile TiO_2 (3.0 eV) was narrower than that of anatase TiO_2 (3.2 eV), and the rutile phase of TiO_2 began to form when the calcination temperature was increased. The E_g of un-doped TiO_2 nanotubes was between 3.30 and 3.22 eV, which was a little higher than that of anatase TiO_2 in powder form. This shift was owing to the quantum size effect on different morphologies of the catalysts [18]. The reflectance spectra of ion-doped TiO_2 slightly shifted toward a longer wavelength (red shift) compared with those of un-doped TiO_2, and the E_g of ion-doped TiO_2 was visibly narrower. The results show that the doped elements were indeed integrated into the lattice of the TiO_2 nanotubes, thereby altering the crystal and electronic structures of the TiO_2 nanotubes [17]. The reduction in E_g of the TiO_2 nanotubes allows the excitation of the catalyst at a lower irradiation power. Thus, the photocatalytic activity of the catalyst is enhanced [19].

Photocatalytic activity tests were conducted to investigate the effects of morphology, calcination temperature, and the type of dopants on the catalytic activity of TiO_2 nanotubes. As shown in Fig. 4, the highest catalytic activity for the un-doped TiO_2 nanotubes was observed at a calcination temperature of 500 °C, with an RB removal efficiency of 98.1%. The S_{BET}, crystalline phases, crystallinity, and E_g of TiO_2 nanotubes were considered as crucial factors that affect the photocatalytic activity of the catalyst. When the calcination temperature was increased, the S_{BET} decreased (see Tabl. 1). The S_{BET} could affect the photocatalytic activities of the catalyst because a larger S_{BET} indicates that more pollutants are adsorbed onto the surface of the catalyst, and more areas become available for electron-hole pair separation. The anatase phase exhibited a higher photocatalytic activity compared with other phases [17]. Although the S_{BET} of TiO_2 nanotubes calcined at 450 °C were larger, the crystalline phases were predominantly amorphous, which resulted in low photocatalytic activity, and broadened E_g of TiO_2. For TiO_2 nanotubes calcined at 550 °C, and 600 °C, although the main crystalline phases were anatase, the amount of rutile phase increased, and the S_{BET} decreased; thus, the overall efficiencies were low.

The first order kinetics equation fitting models were developed to predict removal efficiency using variables (time) (Tabl. 2).

Photocatalytic activity was also affected by ionic radius, valence state, and configuration. The removal of RB increased when Cu^{2+}, V^{5+}, and Zn^{2+} were doped into the TiO_2 nanotubes. The highest photocatalytic activity was obtained in the presence of Zn^{2+}-doped catalyst calcined at 550°C, where 98.7% of RB was removed. The catalytic activity was affected by the following factors. First, the existing impurity band can reduce the recombination of photoinduced electron-hole, which can transfer electrons more efficiently to the oxygen adsorbed on the surface of TiO_2 nanotubes [20]. Second, the weight fractions of the anatase phases of the catalyst were larger than those of un-doped TiO_2 nanotubes, the E_g of the nanotubes were narrower, and the S_{BET} of the catalyst were smaller. Third, the ionic radii of the doped ions affected the photocatalytic activities.

The ionic radii of Cu^{2+} and Zn^{2+}, which were 73 and 74 pm, respectively, were slightly larger than that of Ti^{4+}. CuO and ZnO might be formed on the surface of the TiO_2. In the TiO_2 semiconductors, the potential energy levels of the conduction and valance band of TiO_2 and ZnO lie above the CuOcb and CuOvb levels. Accordingly, the ultraviolet irradiation induces both the e^- transfer and h^+ transfer from TiO_2 and ZnO to CuO [21]. The combination of TiO_2 with the doped metallic oxide results in the generation of Ti^{3+}. The electrons were transferred to $Ti^{3+}$and then to the oxygen, which could reduce the probability for recombination between electrons and holes. In addition, the photogenerated holes left in the valence band would have more opportunity to participate in the oxidizing reactions because photogenerated electrons can be effectively scavenged by Cu^{2+} and Zn^{2+} ions [22]. Therefore, the removal efficiencies increased, with the RB removal efficiency of 98.2% and 98.7% in the presence of 450°C calcined Cu^{2+}-doped and 550°C calcined Zn^{2+}-doped TiO_2.

Doping TiO_2 with V^{5+}, whose valence was higher than that of the parent Ti^{4+}, resulted in an increase in the concentration of electrons in the conduction band. An upward shift of the Fermi energy level was also expected. When the dopant concentration was increased, the surface barrier became higher and the space charge region became narrower [23]. The electron-hole pairs photogenerated within this region were efficiently separated by the large electric field traversing the barrier before these pairs had the chance to recombine [24]. Therefore, the RB removal efficiency increased to be 98.6% when the calcination temperature was 550°C.

4. Conclusions

Ion-doped TiO_2 nanotubes were successfully synthesized for RB removal. The ions were effectively incorporated into the TiO_2 lattice. When the ions were doped and the calcination temperature was increased, the S_{BET} of TiO_2 decreased, and the E_g of ion-doped TiO_2 became visibly narrower. The photocatalytic activities of catalysts on RB removal could be increased when ions were doped into the TiO_2 nanotubes. The Zn^{2+}-doped TiO_2 nanotubes had the highest catalytic activity because of the effects of the weight fractions of the anatase phase, S_{BET}, E_g, and the doped ions.

References

1. Sayılkan, F., Erdemoğlu, S., Asiltürk, M., et al *Mater. Res. Bull.,* **41**(12), 2276, 2006.
2. Lin, C., Lin, K.S., *Chemosphere*, **66**, 1872, 2007.
3. Li, H., Wang, J., Li, H., Yin, S., Sato, T. , *Res. Chem. Interm.,* **36**(1), 27, 2010.
4. Bastakoti, B.P., Wu, K.C., Yamauchi, Y. *J. Nanosci. Nanotechn.*, **13**(4), 2735, 2013.
5. Oveisi, H., Suzuki, N., Beitollahi, A., Yamauchi, Y., *J. Sol-Gel Scie. Techn.*, **56** (2), 212, 2010.
6. Tachikawa, T., Tojo, S., Fujitsuka, M., Toru Sekino, A., Majima, T., *J. Phys. Chem. B*, **110**(29), 14055, 2006.
7. Sun, L., Li, J., Wang, C.L., Li, S.F., Chen, H.B., Lin, C.J., Lin C J., *Solar Energy Mater. Solar Cells,,* **93**, 1875, 2009
8. Zhu, Y., Zhang, L., Yao, W., Cao, L., *Appl. Surf. Scie.*, **158**, 32, 2000.
9. Vásquez, G.C., Pecheherrero, M.A., Maestre, et al, *J.Phys. Chem. C*, **117**(4), 1941, 2013.
10. Spurr, R.A., Myers, H., *Anal. Chem.*, **29**(5), 760, 1957.
11. Pang, Y.L., Abdullah, A.Z., *J. Hazard. Mater.* **235–236**(2), 326, 2012.
12. Ravichandran, L., Selvam, K., Krishnakumar, B., Swaminathan, *J. Hazard. Mater.* **167**(1), 763, 2009.
13. Chang, S.M., Liu, W.S., *Appl. Catal. B Environment.*, **156-157**, 466, 2014.
14. Li, X., Zou, X., Qu, Z., Zhao, Q., Wang, L., *Chemosphere*, **83**(5), 674, 2011.
15. Gomes, Silvaalmeida, G.D., Dekosaka, A.T., Monteirorogero, P., Otacruz, S., SilveiraIkeda, á., Ichikawapetri, T., Siqueira, D.F. *Mater. Res.*, **10**(4), 469, 2007.
16. Zhang, G.W., He, G.H., Xue, W.L., Xu, X.F., Liu, D.N., Xu, Y.H.,, *J, Mol,Catal, A Chem,,* **363-364**, 423, 2012.
17. Pang, Y.L., Abdullah, A.Z., *Ultrasonics Sonochem.*, 19(3), 642, 2012.
18. Zhou, M., Yu, J., Liu, S., Zhai, P., Huang, *Appl. Catal. B Environment.*, **89**(1-2), 160, 2009.
19. Pang, Y.L., Abdullah, A.Z., *Appl. Catal. B Environment.*,**129**(3), 473, 2013.
20. Li, A., Zhao, X., Liu, H., Qu, *J.,Water Res.*, **45**(18), 6131, 2011.
21. Khaki, M.R.D., Sajjadi, B., Raman, A.A.A., Wan, M.A.W.D., Shmshirband, S., *Measurement*, 77, 155, 2016
22. Zang, L., Liu, C.Y., Ren, X.M., *J.Photochem. Photobiol. A Chem.*, **79**(3), 189, 1994.
23. Hidalgo, J.M., Tišler, Z., Kubička, D., Raabova, K., Bulanek, R. , *J. Molec. Catal. A Chem.*, **420**, 178, 2016.
24. Habibi, M.H., Hassanzadeh, A., Mahdavi, S. *J. Photochem.Photobiol. A Chem.*, **172**(1), 89, 2005.